Three-photon polarized entanglement and interference generated using six-wave mixing and polarized dressing atomic coherence control

Lan, Guangchen; Zhang, Siqiang; Xiang, Siwei; Wang, Shucai; Luo, Zhiqiang; Ahmed, Irfan; Zhang, Yanpeng

Published in:
OSA CONTINUUM

Published: 15/11/2019

Document Version:
Final Published version, also known as Publisher's PDF, Publisher's Final version or Version of Record

Published version (DOI):
10.1364/OSAC.2.003153

Publication details:
Lan, G., Zhang, S., Xiang, S., Wang, S., Luo, Z., Ahmed, I., & Zhang, Y. (2019). Three-photon polarized entanglement and interference generated using six-wave mixing and polarized dressing atomic coherence control. *OSA CONTINUUM*, *2*(11), 3153-3164. https://doi.org/10.1364/OSAC.2.003153

Research Article Vol. 2, No. 11 / 15 November 2019 / OSA Continuum 3153

Three-photon polarized entanglement and interference generated using six-wave mixing and polarized dressing atomic coherence control

GUANGCHEN LAN,[1] SIQIANG ZHANG,[1] SIWEI XIANG,[1] SHUCAI WANG,[1] ZHIQIANG LUO,[1] IRFAN AHMED,[2,3] AND YANPENG ZHANG[1,*]

[1] *Key Laboratory for Physical Electronics and Devices of the Ministry of Education & Shaanxi Key Lab of Information Photonic Technique, Xi'an Jiaotong University, Xi'an 710049, China*
[2] *Department of Physics, City University of Hong Kong, Kowloon, Hong Kong SAR, China*
[3] *Department of Electrical Engineering, Sukkur IBA University, 65200, Sindh, Pakistan*
[*] *ypzhang@mail.xjtu.edu.cn*

Abstract: In a spontaneous process, laser-polarized dressings produce characteristic triphoton waveforms regarding the oscillation period and coherence time. Correspondingly, circularly polarized dressings make it have longer oscillation periods compared to the effect of linearly polarized dressings attributed to dispersion relation changes, and shorter coherence times owing to the larger dressing field. Given that the optical response of the polarization state of incident light is the dressing field, we can control the averaged three-photon coincidence count rate by adjusting the polarization of the incident light. By performing quantum tomography, we can obtain W and W-like polarization entanglement states. Accordingly, strong and weak visibilities can be evoked for circularly and linearly polarized dressings.

1. Introduction

Entanglement plays a central role in the field of quantum information as justified by the ongoing efforts for its quantitative and qualitative characterizations [1]. The nonclassical multiphoton is one of the most important parts of entanglement that can be applied in quantum computing [2], communication, imaging technology [3], and in many other fields.

It is known that the most common method used to generate entangled photon pairs is SPDC [4]. The SPDC process occurs in the nonlinear crystal and should meet the phase-matching condition, but the bandwidth of the generated photon pairs can be as high as several of THz with short coherent time.

Biphotons generated from spontaneous parametric down conversion (SPDC) in nonlinear crystals have considerably broad bandwidths (> THz) and ultrashort coherence time (< ps). Using spontaneous four-wave mixing (SFWM) in cold atoms, we can produce narrowband (~ MHz) biphotons with long coherence time (0.1–1.0 μs). This long coherence time allows us to access directly and manipulate the biphoton quantum waveform in the time domain. Du et al. used on-resonance spontaneous four-wave mixing in a hot paraffin-coated ^{87}Rb vapor cell at 63 °C to produce biphotons with controllable bandwidth (1.9–3.2 MHz) and coherence time (47–94 ns) [5].

While entanglement of bipartite systems is well understood [6], the characterization of entanglement for multipartite systems is still intensely investigated. Hübel et al. obtained photon triplets with the use of two cascaded SPDCs [7,8]. Wen [9] theoretically obtained photon triplets via two cascaded, spontaneous four-wave mixing (SFWM) schemes. Ding and his group adopted

#373122 https://doi.org/10.1364/OSAC.2.003153
Journal © 2019 Received 18 Jul 2019; revised 17 Oct 2019; accepted 25 Oct 2019; published 4 Nov 2019

OSA CONTINUUM

a method based on which a spontaneous Raman scattering process in a hot Rb atomic cell cascaded by a SPDC process allowed the realization of the hybrid-cascaded photon triplets [10].

Enhanced four-wave mixing and six-wave mixing [11–13] channels via dual electromagnetically induced transparency windows can be controlled by three nested, parallel, and sequentially cascaded schemes for double dressing [14] in an open, five-level atomic system. The nature of multiphoton correlation comes from the higher order of optical nonlinearity. Our work shows the advantage of the use of polarization dressing [15] to control the three-photon polarization entanglement [16].

In this study, we generate polarization-entangled multiphoton states using spontaneous, parametric, six-wave mixing (SP–SWM), in hot rubidium atomic vapors, which can preserve the entanglement in a longer time than solid media or cascaded process. Then, we control the properties of entangled optics by changing polarized dressing fields. Specifically, we present the three-photon polarization entangled W-like state. The fifth-order nonlinear susceptibility predicted six types of spontaneous six-wave mixings (SSWMs) that occur in this process following the introduction of the polarized dressing field. To further explore the properties of the generated photons, we calculate the triphoton coincidence counting rate using linear and circularly polarized dressing of the employed fields, respectively. We also present the influence of the polarization dressing on the density matrix and interference.

The paper is organized as follows. In Section II, we derive the third-order intensity correlation function with polarization dressings and dressing perturbation chains. In Section III, we discuss the optically polarized entanglement, and present the mechanism of triphoton generation via a nonlinear response in the presence of a polarized dressing field. In Section IV, we apply the polarized dressing in quantum state tomography. In Section V, we discuss the theoretical basis of three-photon interference with polarization entanglement. Finally, in Section VI, we outline the summary and conclusions of this study.

2. Experimental setup

The schematic of the simplified experimental setup in theory is illustrated in Fig. 1(a) in which the SWM process is demonstrated by employing the incident fields on ^{85}Rb atomic vapors. We assume that atoms equally distribute in the basic($|a>5S1/2\ F=3$) Zeeman states. To make the process approximately a steady state, continuous lasers are only used in this theory. We use a strong optical-pumping laser $\boldsymbol{E}_{\mathrm{OP}}$ in Fig. 1(a) to optically pump the atoms from the level $|5S1/2, F=2$ to $|5P1/2, F=2$, to suppress the on-resonance Raman scattering of the coupling beam. So, re-distribution caused by the optical pumping effect may not be obvious enough to influence the calculation. The triphoton generation achieved by a four-level "tri-Λ" atomic system is presented in Fig. 1(f). The four-level atoms are prepared in the base level $|a>$. The medium is confined in a long and narrow cylindrical volumetric shape with length L. In Fig. 1(f), with a detuning of Δ_1, the weak pump beam $\boldsymbol{E}_1$ (wave vector $\boldsymbol{k}_1$, frequency ω_1, Rabi frequency G_1, and a wavelength of 795 nm) is applied to the transition $|a>\rightarrow|c>$. Accordingly, Δ_i=Ω_i-ω_i denotes the detuning, which is defined as the difference between the laser resonant frequency ω_i and the transitional frequency Ω_i of $\boldsymbol{E}_i$. The strong coupling beam $\boldsymbol{E}_2$ ($\boldsymbol{k}_2$, ω_2, G_2, 780 nm) is close to the atomic transitional resonant frequency during the transition $|b>\rightarrow|d>$ with the detuning Δ_2, and counter-propagates to $\boldsymbol{E}_1$. The other coupling beam $\boldsymbol{E}_3$ ($\boldsymbol{k}_3$, ω_3, G_3, 780 nm) propagates in the direction of $\boldsymbol{E}_1$, and is utilized in the atomic transition $|a>\rightarrow|d>$ with the detuning Δ_3. All of the beams are coupled and focused into the center of the Rb vapor by optical lenses. Subsequently, with the phase-match condition $\boldsymbol{k}_1$+$\boldsymbol{k}_2$+$\boldsymbol{k}_3$=$\boldsymbol{k}_{S1}$+$\boldsymbol{k}_{S2}$+$\boldsymbol{k}_{S3}$ and given the low-gain limitation, the SWM process occurs spontaneously. The SWM generate the correlated tripartite $\boldsymbol{E}_{S1}$, $\boldsymbol{E}_{S2}$, and $\boldsymbol{E}_{S3}$, with conserved energy $\omega_1+\omega_2+\omega_3=\omega_{s1}+\omega_{s2}+\omega_{s3}$. From another perspective, polarization directions are also conserved, while the Zeeman energy level matters in circular polarization cases.

OSA CONTINUUM

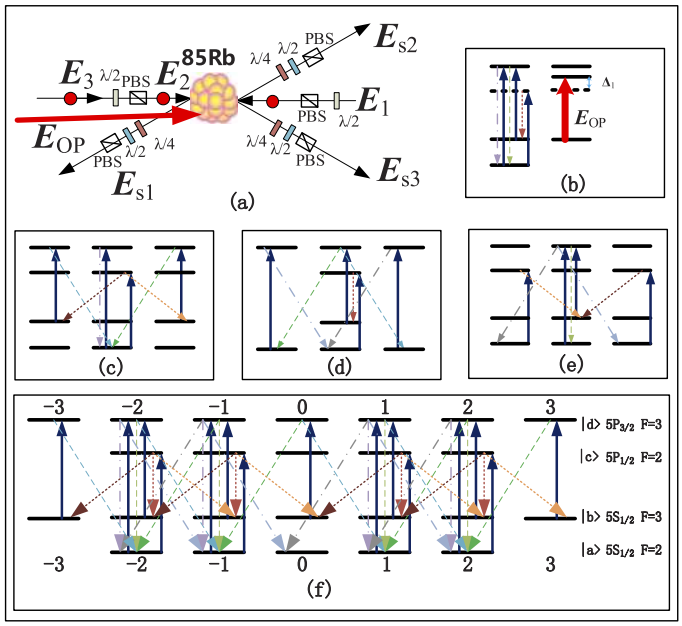

Fig. 1. (a) Schematic diagrams of the experimental arrangement in the ^{85}Rb atomic vapor. $\boldsymbol{E}_{\mathrm{OP}}$ is omitted in (c)–(f). (b)–(f) Zeeman energy level diagrams and transition paths at different laser polarized configurations in four-level systems along with (b)–(e) schematic diagrams of single processes and (f) the schematic diagram of the entire set of processes.

Herein, the employed pump beam is much weaker compared to the coupling beam, far from resonance, and with a large detuning, which leads to reduced quantum atomic noise and retains the atomic population is in the ground state. In addition, the strong coupling beams $\boldsymbol{E}_2$ and $\boldsymbol{E}_3$ in near-resonant relationships form a Λ electromagnetically induced transparency (EIT) scheme. Herein, the coupling beams produce a transparent window for the photons $\boldsymbol{E}_{S2}$ and $\boldsymbol{E}_{S3}$ with a slow-light effect and also assist the SSWM nonlinear process. The generated triphoton could be gauged by three single-photon counting modules (SPCM). Because our theory is based upon the cool atomic ensemble, we do not take the quantum Langevin noise and Doppler broadening into account. We concentrate instead on the interference of the multimode SSWM and the triphoton temporal correlation that is controlled by polarization.

In the description of the interaction, if the reflections from the systematic surfaces are ignored, and the rotating-wave approximation is used, the effective interaction Hamiltonian of the SWM process could be expressed as,

$$H_I = \varepsilon_0 \int_V d^3 z \chi^{(5)} E_1^{(+)} E_2^{(+)} E_3^{(+)} E_{S3}^{(-)} E_{S2}^{(-)} E_{S1}^{(-)} + H.c. \tag{1}$$

where $\chi^{(5)}$ is the fifth-order nonlinear susceptibility of the generated photon field delineated by the nonlinear polarization, V is the interaction volume enlightened by all of the input fields, $H.c$ is the Hermitian conjugate, and $E_1^{(+)}$, $E_2^{(+)}$, and $E_3^{(+)}$, are the positive frequency parts of the input beams which are respectively denoted by the strong classical fields,

$$E_1^{(+)} = E_1 e^{i(\mathbf{k_1 z} - \omega_1 t)}, E_2^{(+)} = E_2 e^{i(\mathbf{k_2 z} - \omega_2 t)}, E_3^{(+)} = E_3 e^{i(\mathbf{k_3 z} - \omega_3 t)}, \tag{2}$$

OSA CONTINUUM

where $E_i = i\sqrt{\hbar\omega_i/2\varepsilon_0 n_i^2 V_q}$, $\mathbf{k_i}$ is the field wavenumber, and V_q is the quantization volume. The generated photons are determined by the quantized fields,

$$E_{S1}^{(+)}(z,t) = \frac{1}{\sqrt{2\pi}}\int d\omega\sqrt{\frac{2\hbar\varpi_{S1}}{c\varepsilon_0 A}}\hat{a}_{S1}(\omega)e^{i[\mathbf{k}_{S1}\mathbf{z}-\omega t]},$$

$$E_{S2}^{(+)}(z,t) = \frac{1}{\sqrt{2\pi}}\int d\omega\sqrt{\frac{2\hbar\varpi_{S2}}{c\varepsilon_0 A}}\hat{a}_{S2}(\omega)e^{-i[\mathbf{k}_{S2}\mathbf{z}+\omega t]},$$

$$E_{S3}^{(+)}(z,t) = \frac{1}{\sqrt{2\pi}}\int d\omega\sqrt{\frac{2\hbar\varpi_{S3}}{c\varepsilon_0 A}}\hat{a}_{S3}(\omega)e^{i[\mathbf{k}_{S3}\mathbf{z}-\omega t]}, \tag{3}$$

where A is the single-mode cross-sectional area, $\hat{a}_{S1}$, $\hat{a}_{S2}$, and $\hat{a}_{S3}$, are the respective photon annihilation operators in the output modes S_1, S_2, and S_3, ε_0 is the vacuum permittivity, c is the speed of light in vacuum, and ϖ_{si} is the central frequency of the generated photon. Substituting the values of the electric fields from Eqs. (2) and (3) in the variables of Eq. (1), Eq. (1) can be rewritten as,

$$\hat{H}_I = W_1\int d\omega_{S1}d\omega_{S2}d\omega_{S3}\kappa\,\mathrm{sin}\,c(\frac{\Delta kL}{2})\hat{a}_{S1}^{\dagger}\hat{a}_{S2}^{\dagger}\hat{a}_{S3}^{\dagger}e^{-i\Delta\omega t} + H.c., \tag{4}$$

where $W_1 = i\sqrt{\hbar^3/\pi^3\varepsilon_0^3 A^3}$ is defined as a constant, $\kappa = -i\sqrt{\varpi_{S1}\varpi_{S2}\varpi_{S3}/c^3}\chi^{(5)}(\omega_{S1},\omega_{S2},\omega_{S3})E_1E_2E_3$ is the nonlinear parametric coupling coefficient, $\Delta k = -k_1 - k_2 - k_3 + k_{S1} + k_{S2} + k_{S3}$ is the phase mismatching down the z–axis, and $\Delta\omega = \omega_1 + \omega_2 + \omega_3 - \omega_{S1} - \omega_{S2} - \omega_{S3}$. When $\Delta k = 0$, conformance with the phase-matching condition is achieved.

On the basis of the first-order perturbation in the interaction plot, we deduce the photon state on the output surface, which is approximately a linear superposition of |Ψ> and |0>, where $|0>$ is the state of vacuum. If there is no influence from the vacuum, we can ignore $|0>$. The photon triplet state |Ψ> could be indicated as,

$$|\psi\rangle = \frac{-i}{\hbar}\int_{-\infty}^{+\infty} dt\,\hat{H}_I|0\rangle. \tag{5}$$

Considering Eqs. (4) and (5), $e^{-i\Delta\omega t}$ turns to $2\pi\delta(\Delta\omega)$, which ensures that i) the energy is conserved during the SSWM process, and ii) frequency entanglement occurs in the triphoton state. Furthermore, Eq. (5) can be changed to,

$$\begin{aligned}|\psi\rangle &= \int d\omega_{S1}d\omega_{S2}d\omega_{S3}\kappa\,\mathrm{sin}\,c(\tfrac{\Delta kL}{2})\hat{a}_{S1}^{\dagger}\hat{a}_{S2}^{\dagger}\hat{a}_{S3}^{\dagger}\delta(\Delta\omega)|0\rangle \\ &= \int d\omega_{S1}d\omega_{S2}d\omega_{S3}\kappa(\omega_i)\,\mathrm{sin}\,c(\tfrac{\Delta kL}{2})\hat{a}_{S1}^{\dagger}\hat{a}_{S2}^{\dagger}\hat{a}_{S3}^{\dagger}|0\rangle\end{aligned}. \tag{6}$$

From Eq. (6), we can predict that the triphoton state is entangled both in terms of the wave number and frequency, and $\kappa(\omega_i) = \kappa(\omega_{S1}, \Delta\omega + \omega_{S2}, \omega_{S3})$ exhibits entanglement in the frequency space, which is the outcome of the energy conservation condition. $sinc(\Delta kL/2)$ is the wave number entanglement, and cannot be factorized into three free-running functions which respectively contain k_{S1}, k_{S2}, and k_{S3}

To discuss the optical characteristics of generated photons in a four-level system, we need to consider the triphoton coincidence counting rate. We arrange the detected photons at the SPCM 1–3 according to the frequencies ω_{S1}, ω_{S2}, and ω_{S3}. Postulating perfect detection efficacy, the

OSA CONTINUUM

mean triphoton coincidence counting rate can be defined by

$$R_{cc} = \lim_{T\to\infty} \frac{1}{T} \int_0^T dt_{S1} \int_0^T dt_{S2} \int_0^T dt_{S3} G^{(3)} M_1(t_{S2} - t_{S1}) M_2(t_{S3} - t_{S1}), \tag{7}$$

where $M_1(t_{S1} - t_{S2})$ and $M_2(t_{S3} - t_{S2})$ are the coincidence window functions. We reckon that $M_1(t_{S1} - t_{S2})$ $|t_{S1} - t_{S2}|<t_{cc}$ for $M_i = 1$, and $M_2(t_{S3} - t_{S2})$ $|t_{S3} - t_{S2}|<t_{cc}$, for $M_i = 0$.

$$G^{(3)} = \left|\langle\Psi| E_{S1}^{(-)} E_{S2}^{(-)} E_{S3}^{(-)} E_{S3}^{(+)} E_{S2}^{(+)} E_{S1}^{(+)} |\Psi\rangle\right| = \left|\langle 0| E_{S3}^{(+)} E_{S2}^{(+)} E_{S1}^{(+)} |\Psi\rangle\right|^2 = |B(\tau_{S1}, \tau_{S2}, \tau_{S3})|^2, \tag{8}$$

where r_{Si} and $\tau_{Si} = t_{Si} - r_{Si}/c$ are the photon's optical path from the output surface from the medium to the detector. For simplicity, we consider that $r_{S1} = r_{S2} = r_{S3}$ and $B(\tau_{s1}, \tau_{s2}, \tau_{s3})$ is the triphoton amplitude. Combining Eqs. (3) and (6), we obtain,

$$B(\tau_{S1}, \tau_{S2}, \tau_{S3}) = W_2 \int d\omega_{S1} d\omega_{S2} d\omega_{S3} \kappa(\omega_i) \Phi(\Delta kL) e^{-i(\omega_{S1}\tau_{S1} + \omega_{S2}\tau_{S2} + \omega_{S3}\tau_{S3})}, \tag{9}$$

where W_2 is a constant which absorbs all of the constants and slow changing terms, and $\Phi(\Delta kL) = sinc(\Delta kL/2) e^{iL(k_{S1}+k_{S2}+k_{S3})/2}$ is the lengthwise detuning function which determines the natural spectral width. Based on Eq. (9), the mode of the triphoton amplitude is determined by both the lengthwise detuning function Φ and the nonlinear parametric coupling coefficient k.

Based on the process depicted in Fig. 1, and according to the theory of odd-ordered nonlinear susceptibilities [17] defined Eq. (10), we can express all the perturbation chains of linearly polarized incident light, which describe the process. Specifically,

$$3xxxxxx = \left(\begin{array}{l} xxxxyy + xxxyyx + xxyyxx + xyyxxx + yyxxxx + yxyxxx + yxxyxx + yxxxyx \\ + yxxxxy + xyxyxx + xyxxyx + xyxxxy + xxyxyx + xxyxxy + xxxyxy \end{array} \right), \tag{10}$$

where x is horizontal polarization and y is vertical polarization.

3. Triphoton response and counting with polarization dressing

Based on the prediction of Eq. (9), the mode of the triphoton amplitude is determined by the lengthwise detuning function and the fifth-order nonlinear susceptibility. Therefore, in this section we pay attention to the nonlinear and linear optical responses of the generated fields.

On the basis of the theory of dressing perturbation chains according to the enhancement of the power of $\boldsymbol{E}_3$, we use a dressing field to change χ. From Table 1, the fifth-order nonlinear susceptibility of the generated fields can be written as

$$\chi_{S3}^{(5)} = \frac{N_0}{d'_{31} d''^{d}_{21} d''_{41} d'^{d}_{11} d'''_{41}} = \frac{N_0}{\varepsilon_0 \hbar (\Gamma_{20} + i\Delta_2) P_3(\delta_2, \delta_3)}, \tag{11}$$

where $N_0 = 2N\mu_{13}\mu_{24}\mu_{14}\mu_{32}\mu_{41}\mu_{41}/\varepsilon_0\hbar^5$ is a constant, μ_{ij} is the electric dipole matrix element, $d''_{41} = \Gamma_{41} - i\delta_1 - i\delta_3 + i\Delta_1$, $d'_{31} = \Gamma_{31} + i\Delta_2$, $d'_{21} = \Gamma_{21} - i\delta_1 - i\delta_3$, $d'_{11} = \Gamma_{11} - i\delta_3$, $d'''_{41} = \Gamma_{41} - i\delta_3 + i\Delta_3$, Γ_{ij} are the dephasing rates of coherence $|j>\rightarrow|i>$, Δ_i=Ω_i-ω_i is the detuning defined as the difference of laser frequency ω_i of $\boldsymbol{E}_i$, and Ω_i is the resonant transitional frequency.

The linear susceptibility of the generated photons is

$$\chi_{s3} = \frac{N_1 \mu_{14}^2}{\ddot{d}_{41}}, \tag{12}$$

where $\ddot{d}_{41} = \Gamma_{41} + i(\Delta_3 + \delta_1 + \delta_2)$, and $N_1 = 2N/\varepsilon_0\hbar$ is a constant.

OSA CONTINUUM

The wave function of the triphoton is a convolution of nonlinear and linear optical responses, and the properties of the triphoton amplitude are determined by both. When the effective coupling Rabi frequency Ω_e and linewidths γ_e are smaller than the phase-matching bandwidth $\Delta\omega_g$, the longitudinal detuning function Φ, which can be approximated to unity represents the linear optical response to the generated fields. Under this circumstance, the nonlinear susceptibility has a major role in the determination of the spectral width. Considering the practical issues, we only concentrate on the nonlinear susceptibility. In such an instance, the coincidence counts of triplets are used to represent a damped Rabi oscillation. Therefore, the effective coupling Rabi frequency Ω_e causes multimode SWM channel occurrence, which generates multimode triphotons.

According to Section II we obtain ${\chi_{Si}}^{(5)}$ and Φ=1. After some mathematical calculations from ${\chi_{S3}}^{(5)}$, the triphoton coincidence counts can be written as,

$$
\begin{aligned}
R_{cc3} = W_2 &\left[\begin{array}{l}
\Omega_{e1}^2 e^{-2(-\Gamma_{10}-\Gamma_{e1})\tau_{12}} + \frac{\Omega_{e1}^2}{2} e^{-2\Gamma_{e1}\tau_{12}}(1-\cos(\Omega_{e1}\tau_{12})) \\
-\Omega_{e1}(-\Gamma_{10}-\Gamma_{e1})\sin(\Omega_{e1}\tau_{12}) \\
+\Omega_{e1}(-\Gamma_{10}-\Gamma_{e1})\sin\left(\left(\frac{\Omega_{e1}}{2}+\frac{\Delta_1}{2}\right)\tau_{12}\right) \\
-\left(\frac{\Omega_{e1}^2}{2}+\left(\frac{\Delta_1}{2}\right)e^{-(-\Gamma_{10}-\Gamma_{e1})\tau_{12}}\right)\cos\left(\left(\frac{\Omega_{e1}}{2}+\frac{\Delta_1}{2}\right)\tau_{12}\right) \\
+\Omega_{e1}(-\Gamma_{10}-\Gamma_{e1})\sin\left(\left(\frac{\Omega_{e1}}{2}-\frac{\Delta_1}{2}\right)\tau_{12}\right) \\
-\left(\frac{\Omega_{e1}^2}{2}-\left(\frac{\Delta_1}{2}\right)e^{-(-\Gamma_{10}-\Gamma_{e1})\tau_{12}}\right)\cos\left(\left(\frac{\Omega_{e1}}{2}-\frac{\Delta_1}{2}\right)\tau_{12}\right)
\end{array}\right] * e^{-2(\Gamma_{e1}\tau_{12}+\Gamma_{e2}\tau_{13})}, \\
* &\left[\begin{array}{l}
\Omega_{e2}^2 e^{-2(\Gamma_{30}-\Gamma_{e2})\tau_{13}} + \frac{\Omega_{e2}^2}{2} e^{-2\Gamma_{e2}\tau_{13}}(1-\cos(\Omega_{e2}\tau_{13})) \\
-\Omega_{e2}(\Gamma_{30}-\Gamma_{e2})\sin(\Omega_{e2}\tau_{13}) \\
+\Omega_{e2}(\Gamma_{30}-\Gamma_{e2})\sin\left(\left(\frac{\Omega_{e2}}{2}-\frac{\Delta_1}{2}-\Delta_3\right)\tau_{13}\right) \\
-\left(\frac{\Omega_{e2}^2}{2}+\left(-\frac{\Delta_1}{2}-\Delta_3\right)e^{-(\Gamma_{30}-\Gamma_{e2})\tau_{13}}\right)\cos\left(\left(\frac{\Omega_{e2}}{2}-\frac{\Delta_1}{2}-\Delta_3\right)\tau_{13}\right) \\
+\Omega_{e2}(\Gamma_{30}-\Gamma_{e2})\sin\left(\left(\frac{\Omega_{e2}}{2}+\frac{\Delta_1}{2}+\Delta_3\right)\tau_{13}\right) \\
-\left(\frac{\Omega_{e2}^2}{2}-\left(-\frac{\Delta_1}{2}-\Delta_3\right)e^{-(\Gamma_{30}-\Gamma_{e2})\tau_{13}}\right)\cos\left(\left(\frac{\Omega_{e2}}{2}+\frac{\Delta_1}{2}+\Delta_3\right)\tau_{13}\right)
\end{array}\right]
\end{aligned}
\tag{13}
$$

where τ_{23}=τ_{S2}-τ_{S3} and τ_{12}=τ_{S1}-τ_{S2}. Clearly, the Rabi oscillation has an oscillation period that results from $2\pi/\Delta_1$ in the direction of τ_{12} and multiple oscillation periods resulting from several sine functions in the direction of τ_{23}.

From the dressing perturbation chains presented in Table 1, we can write down the specific susceptibility of the generated photons.

Regarding the linear polarization, $\theta = 0$,

$$
\begin{aligned}
\chi_{S3M}^{(5)} = &\sum_{M=\pm1,\pm2,\pm3} \frac{2N\mu^6}{\varepsilon_0\hbar} \\
&\times \frac{1}{(\Gamma_{20M}+i\Delta_2)(\Gamma_{10M}-i\delta_1-i\delta_3+\frac{CG^2G_{1M}^2(\cos^4\theta+\sin^4\theta)}{\Gamma_{30M}-i\delta_1-i\delta_3-i\Delta_1})} \\
&\frac{}{(\Gamma_{30M}-i\delta_1-i\delta_3+i\Delta_1)(\Gamma_{00M}-i\delta_3+\frac{CG^2G_1^2(\cos^4\theta+\sin^4\theta)}{\Gamma_{11M}-i\delta_3-i\Delta_1})(\Gamma_{30M}-i\delta_3+i\Delta_3)}
\end{aligned}
\tag{14}
$$

Ω_{e3} and Ω_{e2} in R_{cc3} need to be rewritten as,

$$
\begin{aligned}
\Omega_{e1} &= \sqrt{[\Delta_1^2 + 4((\cos^4\theta+\sin^4\theta)(CG_{lin}G_1)^2 + \Gamma_{10}\Gamma_{30})]}, \\
\Omega_{e2} &= \sqrt{[\Delta_1^2 + 4((\cos^4\theta+\sin^4\theta)(\mathrm{C}G_{lin}G_1)^2 + \Gamma_{00}\Gamma_{11})]}.
\end{aligned}
\tag{15}
$$

OSA CONTINUUM

Table 1. Dressing Perturbation chains of the four-level system for linear and circular polarization configurations for the laser

P polarization (χ_{xccccc})	$\rho_{a_M a_M} \xrightarrow{G^0_{ac}} \rho_{c_M a_M} \xrightarrow{G^0_{cb}} \rho_{b_M a_M} \xrightarrow{G^0_{bd}} \rho_{d_M a_M} \xrightarrow{G^0_{da}} \rho_{a_M a_M} \xrightarrow{G^0_{ad}} \rho_{d_M a_M}\ (M=-2,-1,0,1,2)$ $\rho_{a_M a_M} \xrightarrow{(G^0_{ac})^*} \rho_{a_M c_M} \xrightarrow{G^0_{cb}} \rho_{a_M b_M} \xrightarrow{(G^0_{bd})^*} \rho_{a_M d_M} \xrightarrow{G^0_{da}} \rho_{a_M a_M} \xrightarrow{(G^0_{ad})^*} \rho_{a_M d_M}\ (M=-2,-1,0,1,2)$
P polarization (χ_{xyyyyx})	$\rho_{a_M a_M} \xrightarrow{G^0_{ac}} \rho_{c_M a_M} \xrightarrow{G^{+1}_{cb}} \rho_{b_{M+1} a_M} \xrightarrow{G^0_{bd}} \rho_{d_{M+1} a_M} \xrightarrow{G^{-1}_{da}} \rho_{a_M a_M} \xrightarrow{G^0_{ad}} \rho_{d_M a_M}\ (M=-2,-1,0,1)$ $\rho_{a_M a_M} \xrightarrow{(G^0_{ac})^*} \rho_{a_M c_M} \xrightarrow{G^{+1}_{cb}} \rho_{a_M b_{M+1}} \xrightarrow{(G^0_{bd})^*} \rho_{a_M d_{M+1}} \xrightarrow{G^{-1}_{da}} \rho_{a_M a_M} \xrightarrow{(G^0_{ad})^*} \rho_{a_M d_M}\ (M=-2,-1,0,1)$ $\rho_{a_M a_M} \xrightarrow{G^0_{ac}} \rho_{c_M a_M} \xrightarrow{G^{-1}_{cb}} \rho_{b_{M-1} a_M} \xrightarrow{G^0_{bd}} \rho_{d_{M-1} a_M} \xrightarrow{G^{+1}_{da}} \rho_{a_M a_M} \xrightarrow{G^0_{ad}} \rho_{d_M a_M}\ (M=-1,0,1,2)$ $\rho_{a_M a_M} \xrightarrow{(G^0_{ac})^*} \rho_{a_M c_M} \xrightarrow{G^{-1}_{cb}} \rho_{a_M b_{M-1}} \xrightarrow{(G^0_{bd})^*} \rho_{a_M d_{M-1}} \xrightarrow{G^{+1}_{da}} \rho_{a_M a_M} \xrightarrow{(G^0_{ad})^*} \rho_{a_M d_M}\ (M=-1,0,1,2)$
S polarization (χ_{xxxyxy})	$\rho_{a_M a_M} \xrightarrow{G^0_{ac}} \rho_{c_M a_M} \xrightarrow{G^0_{cb}} \rho_{b_M a_M} \xrightarrow{G^0_{bd}} \rho_{d_M a_M} \xrightarrow{G^{+1}_{da}} \rho_{a_{M+1} a_M} \xrightarrow{G^0_{ad}} \rho_{d_{M+1} a_M}\ (M=-2,-1,0,1,2)$ $\rho_{a_M a_M} \xrightarrow{(G^0_{ac})^*} \rho_{a_M c_M} \xrightarrow{G^0_{cb}} \rho_{a_M b_M} \xrightarrow{(G^0_{bd})^*} \rho_{a_M d_M} \xrightarrow{G^{+1}_{da}} \rho_{a_M a_{M+1}} \xrightarrow{(G^0_{ad})^*} \rho_{a_M d_{M+1}}\ (M=-2,-1,0,1,2)$ $\rho_{a_M a_M} \xrightarrow{G^0_{ac}} \rho_{c_M a_M} \xrightarrow{G^0_{cb}} \rho_{b_M a_M} \xrightarrow{G^0_{bd}} \rho_{d_M a_M} \xrightarrow{G^{-1}_{da}} \rho_{a_{M-1} a_M} \xrightarrow{G^0_{ad}} \rho_{d_{M-1} a_M}\ (M=-2,-1,0,1,2)$ $\rho_{a_M a_M} \xrightarrow{(G^0_{ac})^*} \rho_{a_M c_M} \xrightarrow{G^0_{cb}} \rho_{a_M b_M} \xrightarrow{(G^0_{bd})^*} \rho_{a_M d_M} \xrightarrow{G^{-1}_{da}} \rho_{a_M a_{M-1}} \xrightarrow{(G^0_{ad})^*} \rho_{a_M d_{M-1}}\ (M=-2,-1,0,1,2)$
S polarization (χ_{xyxxxy})	$\rho_{a_M a_M} \xrightarrow{G^0_{ac}} \rho_{c_M a_M} \xrightarrow{G^{+1}_{cb}} \rho_{b_{M+1} a_M} \xrightarrow{G^0_{bd}} \rho_{d_{M+1} a_M} \xrightarrow{G^0_{da}} \rho_{a_{M+1} a_M} \xrightarrow{G^0_{ad}} \rho_{d_{M+1} a_M}\ (M=-2,-1,0,1)$ $\rho_{a_M a_M} \xrightarrow{(G^0_{ac})^*} \rho_{a_M c_M} \xrightarrow{G^{+1}_{cb}} \rho_{a_M b_{M+1}} \xrightarrow{(G^0_{bd})^*} \rho_{a_M d_{M+1}} \xrightarrow{G^0_{da}} \rho_{a_M a_{M+1}} \xrightarrow{(G^0_{ad})^*} \rho_{a_M d_{M+1}}\ (M=-2,-1,0,1)$ $\rho_{a_M a_M} \xrightarrow{G^0_{ac}} \rho_{c_M a_M} \xrightarrow{G^{-1}_{cb}} \rho_{b_{M-1} a_M} \xrightarrow{G^0_{bd}} \rho_{d_{M-1} a_M} \xrightarrow{G^0_{da}} \rho_{a_{M-1} a_M} \xrightarrow{G^0_{ad}} \rho_{d_{M-1} a_M}\ (M=-1,0,1,2)$ $\rho_{a_M a_M} \xrightarrow{(G^0_{ac})^*} \rho_{a_M c_M} \xrightarrow{G^{-1}_{cb}} \rho_{a_M b_{M-1}} \xrightarrow{(G^0_{bd})^*} \rho_{a_M d_{M-1}} \xrightarrow{G^0_{da}} \rho_{a_M a_{M-1}} \xrightarrow{(G^0_{ad})^*} \rho_{a_M d_{M-1}}\ (M=-1,0,1,2)$

In addition, for circular polarization, $\theta = \pm 45^0$,

$$\chi^{(5)}_{S3M} = \sum_{M=\pm1,\pm2,\pm3} \frac{2N\mu^6}{\varepsilon_0\hbar} \times \frac{1}{(\Gamma_{20M}+i\Delta_2)(\Gamma_{10M}-i\delta_1-i\delta_3+\frac{CG^2G^2_{1M}(2\cos^2\theta*\sin^2\theta)}{\Gamma_{30M}-i\delta_1-i\delta_3-i\Delta_1})(\Gamma_{30M}-i\delta_3+i\Delta_3)} \\ (\Gamma_{30M}-i\delta_1-i\delta_3+i\Delta_1)(\Gamma_{00M}-i\delta_3+\frac{CG^2G^2_1(2\cos^2\theta*\sin^2\theta)}{\Gamma_{11M}-i\delta_3-i\Delta_1}) \tag{16}$$

Similarly, Ωe3 and Ωe2 in Rcc3 can be rewritten as,

$$\Omega_{e1} = \sqrt{[\Delta_1^2 + 4((2\cos^2\theta * \sin^2\theta)(\mathrm{CG}_{cir}G_1)^2 + \Gamma_{10}\Gamma_{30})]} \\ \Omega_{e2} = \sqrt{[\Delta_1^2 + 4((2\cos^2\theta * \sin^2\theta)(\mathrm{CG}_{cir}G_1)^2 + \Gamma_{00}\Gamma_{11})]}. \tag{17}$$

CG_{lin} is the coefficient in line polarization which is equal to $\sqrt{5}/6$ when $\theta = 0$ and CG_{cir} is the coefficient in circular polarization which is equal to $5\sqrt{5}/6$ when $\theta = \pm\pi/4$ in the protocol.

As it is shown in Fig. 2, not only the peak values are changed, but also the positions are transformed. Transparently, the peaks are clustered in a linear polarization configuration in Fig. 2(a), whereas they scatter in a circular polarization scheme in Fig. 2(c). From Eq. (14), we know that the roots of χ=0 are clustered around one stable peak. This is caused by the effect of the linearly polarized dressing field which makes the denominator smaller. The peaks appear to be narrower because of the same reason, while the outcomes attributed to Eq. (16) are opposite.

Thus, we deliberate the circumstance to achieve the mixture of phase matchings and the fifth-order nonlinear susceptibility. As shown in Fig. 2(a1), an incisive peak arises close to the origin of the coordinates. When the counting time is increased, the slow lights begin to adjust the wave packet of the triphoton counting rates. The circumstances are the same in Figs. 2(a1)

OSA CONTINUUM

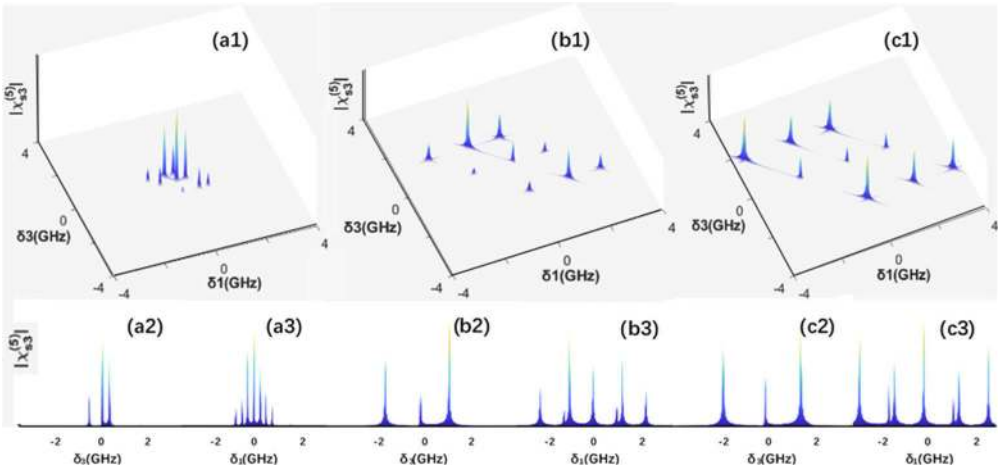

Fig. 2. Resonances in the fifth-order nonlinear susceptibility $|\chi_{S3}{}^{(5)}|$ (a) with a linear polarization dressing field, (b) with dressing field $|G_1|^2$ (without polarization dressing), and (c) with a circular polarization dressing field. (a2), (b2), and (c2), are resonances in the dimension of δ_3 from (a1), (b1), and (c1), respectively. Similarly, (a3), (b3), and (c3), are resonances in the dimension of δ_1 from (a1), (b1), and (c1), respectively.

and 2(b1). Since the CG coefficients may be different for different transitions between Zeeman sublevels, the Rabi frequency can vary with polarization even the frequency and power of the laser field keep unchanged. For example, the CG coefficients, CG_{cir} (circular polarization) and CG_{lin} (linear polarization) are $5\sqrt{5}/6$ and $\sqrt{5}/6$, respectively with M = 1/2. So, the dressing terms in Eq. (17) are $CG^2_{2,lin}(\cos^4\theta + \sin^4\theta)|G_2|^2$ and $CG^2_{2,cir}(2\cos^2\theta\sin^2\theta)|G_2|^2$, respectively. Thus, the ratio between dressing term of circular and linear case is expressed as $CG^2_{2,cir}/CG^2_{2,lin} = 25$, with θ=45° and M=+1/2, which indicates that the dressing effects in the circularly polarized subsystems are far greater than that in the linearly polarized.

As shown in Fig. 3(a–c), we can demonstrate the theoretical curves of the triphoton coincidence counting rate in a damped Rabi oscillation regime by applying different trigger photons at different polarization states. The periods are obviously changed, and are shorter in the circular polarization case and longer in the linear polarization case. It can be observed that when we apply $\boldsymbol{Es}3$ to trigger the photons, the Rabi oscillation only has one oscillation period in the direction τ_{13} because of the monotonic attenuation in Fig. 3, while multiple oscillation periods exist in the direction τ_{23} because of the up and down waves in Fig. 3. If we observe the functions in Eqs.

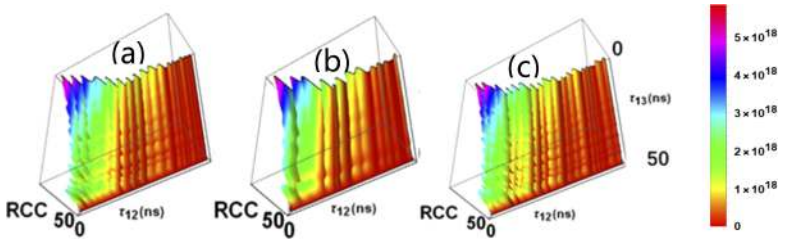

Fig. 3. Multimode triphoton coincidence counting rate in the τ_{12}=t_1-t_2 and τ_{13}=t_1-t_3 directions for the damped Rabi oscillation regime. (a) Without polarized dressing, (b) with linearly polarized dressing, and (c) with circularly polarized dressing fields.

OSA CONTINUUM

(13–17), we can arrive at these conclusions earlier. Accordingly, the value of Ω in the circularly dressed polarization scheme is larger, while it is smaller in the linearly dressed polarization scheme. Based on these equations, the more distant the peaks are in Fig. 2(a1, b1, c1), the shorter are the periods in coincidence counting in Fig. 3. Moreover, the wider the peaks are, the faster are their attenuations in Fig. 3.

As it can be observed, $Rcc_{s3} \propto G_{s3}$, and $B_{s3} \propto \kappa_{s3} \propto \chi_{s3}$. Based on the use of Eq. (8), we obtain $Rcc_{s3} \propto |\chi_{s3}|^2$. Accordingly, we conclude that $Rcc = \sum Rcc_i \propto \sum |\chi_{\mathrm{i}}|^2$. This is why the R_{cc3} equation which is based on a single $\chi_{\mathrm{S3}}{}^{(5)}$ could present the whole properties.

In the next section, we discuss the W and W-like states of the polarization entanglement based on a quantum tomography paradigm.

4. Triphoton quantum tomography

To achieve the full characterization of the gained state, quantum state tomography was conducted [18]. Regarding the three-qubit tomography, 64 projective measurements were required. The output mode was projected on the bases $|V\rangle$ (vertical linear polarization) and $|H\rangle$ (horizontal linear polarization) for each measurement. Each measurement is conducted by embedding a polarizer and a quarter-wave plate in each output mode, and by laying their axes appropriately. The reconstructed density matrix is shown in Fig. 4. It can be obviously observed that within the diagonal parts, $|VVV\rangle_{abc}\langle VVV|$, $|HVH\rangle_{abc}\langle HVH|$, $|HHV\rangle_{abc}\langle HHV|$, and $|VHH\rangle_{abc}\langle VHH|$, are dominant. Within the off-diagonal parts, the cross terms of the dominant diagonal parts are dominant. All the facts show that the four terms $|VVV\rangle_{abc}$, $|HVH\rangle_{abc}$, $|HHV\rangle_{abc}$, and $|VHH\rangle_{abc}$, are well superimposed, while the other terms can be ignored. Quarter, half-wave plate $(h_{1,v}, q_{1,v}, h_{2,v}, q_{2,v}, h_{3,v}, q_{3,v})$ and PBS determine the projection states of the three beams $|\psi_v\rangle$, and they determine the coincidence counting $n_v = N\langle\psi_v|\hat{\rho}|\psi_v\rangle$.

$$\begin{aligned}
|\psi^{(3)}_{proj}\rangle &= |\psi^{(1)}_{proj}(h_1,q_1)\rangle \otimes |\psi^{(1)}_{proj}(h_2,q_2)\rangle \otimes |\psi^{(1)}_{proj}(h_3,q_3)\rangle \\
&= a(h_1,q_1)a(h_2,q_2)a(h_3,q_3)|HHH\rangle + a(h_1,q_1)a(h_2,q_2)b(h_3,q_3)|HHV\rangle \\
&+a(h_1,q_1)b(h_2,q_2)a(h_3,q_3)|HVH\rangle + b(h_1,q_1)a(h_2,q_2)a(h_3,q_3)|VHH\rangle \\
&+b(h_1,q_1)b(h_2,q_2)a(h_3,q_3)|VVH\rangle + a(h_1,q_1)b(h_2,q_2)b(h_3,q_3)|HVV\rangle \\
&+b(h_1,q_1)a(h_2,q_2)b(h_3,q_3)|VHV\rangle + b(h_1,q_1)b(h_2,q_2)b(h_3,q_3)|VVV\rangle.
\end{aligned} \tag{18}$$

Based on the above, we can formulate the density matrix with linear and circular polarized dressings.

For linear polarization,

$$n_{v,lin} = N_{lin}\langle\psi_v|\hat{\rho}|\psi_v\rangle \propto |\chi^{(5)}_{S3M}|^4{}_{\theta=0}. \tag{19}$$

For circular polarization,

$$n_{v,cir} = N_{cir}\langle\psi_v|\hat{\rho}|\psi_v\rangle \propto |\chi^{(5)}_{S3M}|^4{}_{\theta=\frac{\pi}{4}}. \tag{20}$$

Because $\chi^{(5)}_{S3M}$ is influenced by the polarization dressing, n is also influenced. Thus, $n_{v,cir}$ is larger and $n_{v,lin}$ is smaller with respect to each other. In the next subsection, we focus on the direction of polarization.

As shown in Fig. 4(a), in the first panel, when the input optics are HHH, the output is a W-like state as predicted from Eq. (21). In Fig. 4(b), when we change the input optics into HHV, HVH, or VHH, the output is a W-state, as predicted from Eq. (22).

OSA CONTINUUM

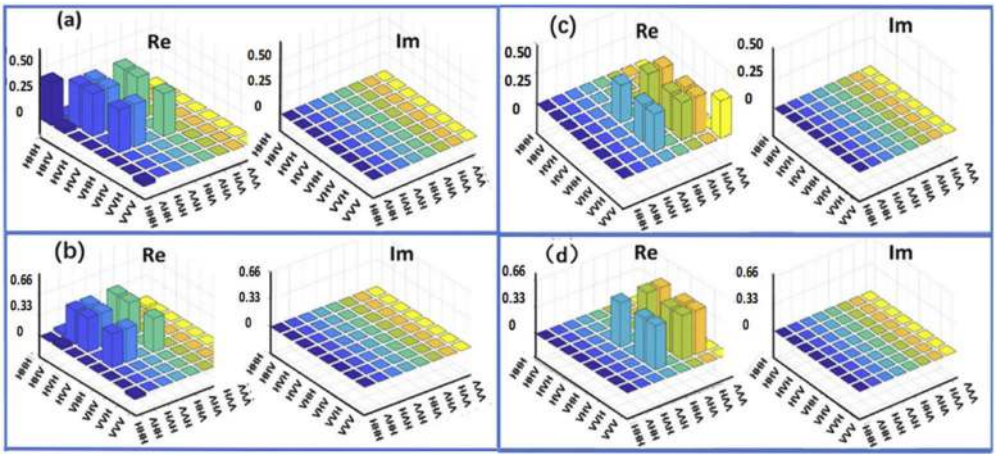

Fig. 4. Reduced density matrix. (a) Input of HHH (W-like state, heights = 1/4). (b) Input of HHV, HVH, or VHH (W-states, heights = 1/3). (c) Input of VVV (W-like state, heights = 1/4). (d) Input of VVH, VHV, or HVV (W-states, heights = 1/3).

As shown in Fig. 4(c), when the input optics are VVV in the second system, the output is in W-like state, as indicated by Eq. (23). Similarly, as shown in Fig. 4(d), when we change the input optics in VVH, VHV, or HVV, the output is in W-state, as indicated by Eq. (24).

$$|W_{11}\rangle = \frac{1}{2}(|HHH\rangle + |VVH\rangle + |HVV\rangle + |VHV\rangle) \tag{21}$$

$$|W_{12}\rangle = \frac{1}{\sqrt{3}}(|HHV\rangle + |HVH\rangle + |VHH\rangle) \tag{22}$$

$$|W_{21}\rangle = \frac{1}{2}(|VVV\rangle + |HHV\rangle + |VHH\rangle + |HVH\rangle) \tag{23}$$

$$|W_{22}\rangle = \frac{1}{\sqrt{3}}(|VVH\rangle + |VHV\rangle + |HVV\rangle) \tag{24}$$

Thus, the proportion of the basic states is changed by polarization, and the outcome state is unique for the specific input. From the above discussion, we can infer that the circular polarized dressing can improve the measurement by approximately 1/3 in the W-state and by 1/4 in the W-like state.

In the next section, we discuss the interference visibility that is controlled by the polarization dressing.

5. Interference with polarized dressing

By considering the influence from the coincidence counting rate, and by setting the strongest (circular polarization) interference visibility as the standard, we can modify the interference equation with polarized dressing according to Eq. (25–27) and θ is the degree of $\lambda/4$ wave plate.

OSA CONTINUUM

Without the polarized dressing,

$$P = \frac{1}{2} + \frac{1}{2}\sqrt{\frac{\iint R_{cc1}\mathrm{d}\tau_{12}\mathrm{d}\tau_{13}}{\iint R_{cc3}\mathrm{d}\tau_{12}\mathrm{d}\tau_{13}}}\cos(\varphi_1 + \varphi_2 + \varphi_3) \tag{25}$$

When $\theta = 0$, in linear polarization,

$$P_{lin} = \frac{1}{2} + \frac{1}{2}\sqrt{\frac{\iint R_{cc2}\mathrm{d}\tau_{12}\mathrm{d}\tau_{13}}{\iint R_{cc3}\mathrm{d}\tau_{12}\mathrm{d}\tau_{13}}}\cos(\varphi_1 + \varphi_2 + \varphi_3) \tag{26}$$

When $\theta = \pi/4$, in circular polarization,

$$P_{cir} = \frac{1}{2} + \frac{1}{2}\cos(\varphi_1 + \varphi_2 + \varphi_3) \tag{27}$$

In Fig. 5, we simulate the normal coincidence counts of the interference of the W-like states (W_{11} and W_{21}) by changing φ_3, which is the degree of the halfwave plate in the $\boldsymbol{E_{s3}}$ tunnel. Accordingly, φ_1 and φ_2 are the degrees of the wave plates in the $\boldsymbol{E_{s1}}$ and $\boldsymbol{E_{s2}}$ tunnel, respectively. In the two simulation conditions we use $\varphi_1 = \varphi_2 = 0$ to detect $|HHH\rangle$ and $\varphi_1 = \varphi_2 = \pi$ to detect $|VVV\rangle$. As it can be observed, the circular interference has the strongest coincidence counts. On the contrary, the linear interference is the weakest. According to $(P_{\max} - P_{\min})/(P_{\max} + P_{\min})$, the circular polarization dressing has a stronger interference visibility than the one without polarization (0.581) which is entangled. Therefore, it should also violate the Bell inequality and is an entangled state. Ideally it is almost equal to unity. However, regarding the linear polarization dressing, the interference visibility is only 0.110. In summary, we changed the intensity of the interference visibility with polarization dressing.

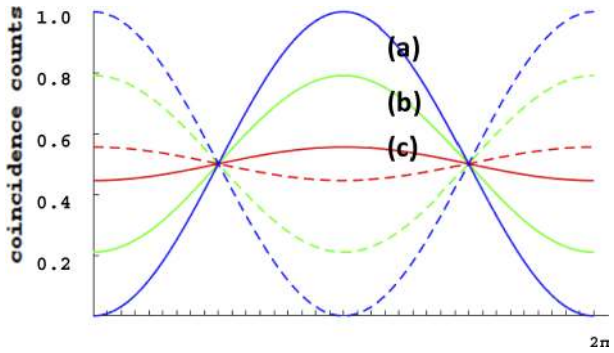

Fig. 5. Interference of normal coincidence counts. (a) With circular polarization, and (b) without polarized dressing. (c) With linear polarization dressing. Dashed lines and solid lines exhibit π phase differences.

Hence, by changing the input optics polarization, we can control the output optics to achieve changes between the W-like and the W states. Furthermore, circular and linear polarizations can each strengthen and weaken the amplitudes of vibration that satisfy the entanglement criteria, $|GHZ\rangle = (|HHH\rangle + |VVV\rangle)/\sqrt{2}$. In comparison to the GHZ state, the W state exhibits perfect correlations and violates the three-particle Mermin inequality, while two-particle entanglement can be observed after the measurement on one of the particles, contrary to the GHZ state [1]. From this viewpoint, the W and W-like states are more entangled and robust.

OSA CONTINUUM

6. Conclusion

In conclusion, we discussed the optical responses of fifth-order nonlinear susceptibility ($\chi_{Si}^{(5)}$) fields generated in the atomic ensemble of SSWM. The process produced seven types of SWM following the introduction of polarized dressing fields. To further explore the entangled properties of the generated photons, we calculated the triphoton coincidence counting rate using linearly and circularly polarized dressings. We also showed the transformation between the W and W-like states by changing the incident light field polarization. Finally, we optimized the density matrix and interference visibility with such polarized dressings. These results could be of great significance for performing fundamental tests of quantum mechanics and quantum information technologies.

Funding

National Key R&D Program of China (2017YFA0303700, 2018YFA0307500); National Natural Science Foundation of China (11604256, 11804267, 11904279, 61605154, 61975159).

Disclosures

The authors declare that there are no conflicts of interest related to this article.

References

1. M. Eibl, N. Kiesel, M. Bourennane, C. Kurtsiefer, and H. Weinfurter, "Experimental realization of a three-qubit entangled W state," Phys. Rev. Lett. **92**(7), 077901 (2004).
2. A. Steane, "Quantum computing," Rep. Prog. Phys. **61**(2), 117–173 (1998).
3. L. A. Lugiato, A. Gatti, and E. Brambilla, "Quantum image," J. Opt. B: Quantum Semiclassical Opt. **4**(3), S176–S183 (2002).
4. H. Hübel, D. R. Hamel, A. Fedrizzi, S. Ramelow, K. J. Resch, and T. Jennewein, "Direct generation of photon triplets using cascaded photon-pair sources," Nature **466**(7306), 601–603 (2010).
5. C. Shu, P. Chen, T. K. A. Chow, L. B. Zhu, Y. H. Xiao, M. M. T. Loy, and S. W. Du, "Subnatural-linewidth biphotons from a Doppler-broadened hot atomic vapour cell," Nat. Commun. **7**(1), 12783 (2016).
6. B. Zhao, Z. B. Chen, Y. A. Chen, J. Schmiedmayer, and J. W. Pan, "Robust creation of entanglement between remote memory qubits," Phys. Rev. Lett. **98**(24), 240502 (2007).
7. L. K. Shalm, D. R. Hamel, Z. Yan, C. Simon, K. J. Resch, and T. Jennewein, "Three-photon energy–time entanglement," Nat. Phys. **9**(1), 19–22 (2013).
8. J. M. Wen, E. Oh, and S. W. Du, "Tripartite entanglement generation via four-wave mixings: narrowband triphoton W state," J. Opt. Soc. Am. B **27**(6), A11–A20 (2010).
9. S. W. Du, J. M. Wen, M. H. Rubin, and G. Y. Yin, "Four-wave mixing and biphoton generation in a two-level system," Phys. Rev. Lett. **98**(5), 053601 (2007).
10. D. S. Ding, W. Zhang, S. Shi, Z. Y. Zhou, Y. Li, B. S. Shi, and G. C. Guo, "Experimental generation of tripartite telecom photons by using an atomic ensemble and a nonlinear waveguide," Optica **2**(7), 642–645 (2015).
11. D. Zhang, Y. Q. Zhang, X. H. Li, D. Zhang, L. Cheng, C. B. Li, and Y. P. Zhang, "Generation of high-dimensional energy-time-entangled photon pairs," Phys. Rev. A **96**(5), 053849 (2017).
12. D. Zhang, C. B. Li, Z. Y. Zhang, Y. Q. Zhang, Y. P. Zhang, and M. Xiao, "Enhanced intensity-difference squeezing via energy-level modulations in hot atomic media," Phys. Rev. A **96**(4), 043847 (2017).
13. X. H. Li, D. Zhang, D. Zhang, L. Hao, H. X. Chen, Z. G. Wang, and Y. P. Zhang, "Dressing control of biphotons waveform transition," Phys. Rev. A **97**, 053830 (2018).
14. Z. Q. Nie, H. B. Zheng, P. Z. Li, Y. M. Yang, Y. P. Zhang, and M. Xiao, "Interacting multiwave mixing in a five-level atomic system," Phys. Rev. A **77**(6), 063829 (2008).
15. C. Shu, X. X. Guo, P. Chen, M. M. T. Loy, and S. W. Du, "Narrowband biphotons with polarization-frequency-coupled entanglement," Phys. Rev. A **91**(4), 043820 (2015).
16. H. Yan, S. C. Zhang, J. F. Chen, M. M. T. Loy, G. K. L. Wong, and S. W. Du, "Generation of narrow-band hyperentangled nondegenerate paired photons," Phys. Rev. Lett. **106**(3), 033601 (2011).
17. Y. Q. Yan, Z. K. Wu, J. H. Si, L. H. Yan, Y. Q. Zhang, C. Z. Yuan, J. Sun, and Y. P. Zhang, "Investigation of odd-order nonlinear susceptibilities in atomic vapors," Ann. Phys. **333**, 307–322 (2013).
18. V. Boyer, A. M. Marino, R. C. Pooser, and P. D. Lett, "Entangled images from four-wave mixing," Science **321**(5888), 544–547 (2008).